Supplementary Information

Electrospun magnetic nanoparticle-decorated nanofiber filter and its applications to high-efficiency air filtration

Juyoung Kim,[1,2,†] Seung Chan Hong,[3,†] Gwi Nam Bae,[1] and Jae Hee Jung[1,4,5,*]

[1]Center for Environment, Health, and Welfare Research, Korea Institute of Science and Technology (KIST), Seoul 02792, Republic of Korea

[2]Department of Chemical Engineering, University of Seoul, Seoul 02504, Republic of Korea

[3]Department of Mechanical and Aerospace Engineering, Seoul National University, Seoul 08826, Republic of Korea

[4]Division of Energy & Environment Technology, KIST School, Korea University of Science and Technology, Seoul 02792, Republic of Korea

[5]Green School, Korea University, Seoul 02841, Republic of Korea

[†] These authors equally contributed to this work.

*Correspondence should be addressed to: jaehee@kist.re.kr; Tel.: 82-2-958-5718

Number of pages: 11 (w/o cover)

Number of figures: 8

Number of tables: 5

Table S1. Measured physical properties of the ethanolic PVP solution (15 wt%) with various Fe_3O_4 MNP concentrations.

MNP Concentration	Density (g/mL)	Conductivity (µS/cm)	Surface tension (mN/m)	Viscosity (Pa·s)
0 wt% (control)	0.8 ± 0.02	1.0 ± 0.04	22.33 ± 0.05	0.51 ± 0.001
5 wt%	0.8 ± 0.02	1.0 ± 0.06	22.50 ± 0.03	0.52 ± 0.001
10 wt%	0.8 ± 0.02	1.1 ± 0.01	22.58 ± 0.03	0.53 ± 0.002
20 wt%	0.8 ± 0.03	1.1 ± 0.05	22.67 ± 0.02	0.54 ± 0.002

Table S2. Pore size distributions of the control and MNP-NF filters.

MNP Concentration	Geometric mean diameter (µm)	Geometric standard deviation
0 wt% (control)	6.2 ± 0.04	1.36 ± 0.008
5 wt%	7.4 ± 0.12	1.38 ± 0.018
10 wt%	9.6 ± 0.18	1.43 ± 0.023
20 wt%	11.1 ± 0.25	1.44 ± 0.026

Table S3. Size characteristics of test airborne metal oxide dust (Fe_2O_3).

Statistics	Values
Mode diameter (nm)	50.7 ± 1.21
Geometric mean diameter (nm)	42.5 ± 3.68
Geometric standard deviation	1.7 ± 0.01
Total concentration (#/cm^3)	~2.43 × 10^4

Table S4. Particle collection efficiency (%) of control and MNP-NF filters at dust sizes of 54, 101, 202, and 300 nm.

MNP Concentration	Particle diameter (nm)			
	54	101	202	300
0 wt% (control)	86 ± 0.8	79 ± 1.0	73 ± 1.1	73 ± 1.0
5 wt%	91 ± 0.7	89 ± 0.9	84 ± 1.5	85 ± 3.5
10 wt%	94 ± 0.5	93 ± 0.9	91 ± 1.0	91 ± 1.9
20 wt%	98 ± 0.5	97 ± 0.3	96 ± 1.3	97 ± 3.6

Table S5. Chemical composition of subway dust, determined using XRF. The mass concentration of elements in the subway dust was obtained using XRF and calculated in the form of oxide compounds. The most abundant component was iron oxide (Fe_2O_3), with a concentration of 68.9 wt%. The results indicate that the subway dust has strong magnetic susceptibility.

No.	Component	Concentration (wt%)
1	Fe_2O_3	68.9
2	C	10.5
3	SiO_2	7.28
4	Al_2O_3	4.21
5	CaO	4.07
6	SO_3	1.33
7	CuO	0.779
8	MgO	0.585
9	MnO	0.54
10	N	0.357
11	BaO	0.31
12	ZnO	0.237
13	K2O	0.218
14	TiO_2	0.151
15	Cr_2O_3	0.143
16	Na_2O	0.0939
17	ZrO_2	0.086
18	P_2O_5	0.0846
19	Cl	0.0684
20	NiO	0.0292
21	PbO	0.0199
22	SrO	0.0192

Figure S1

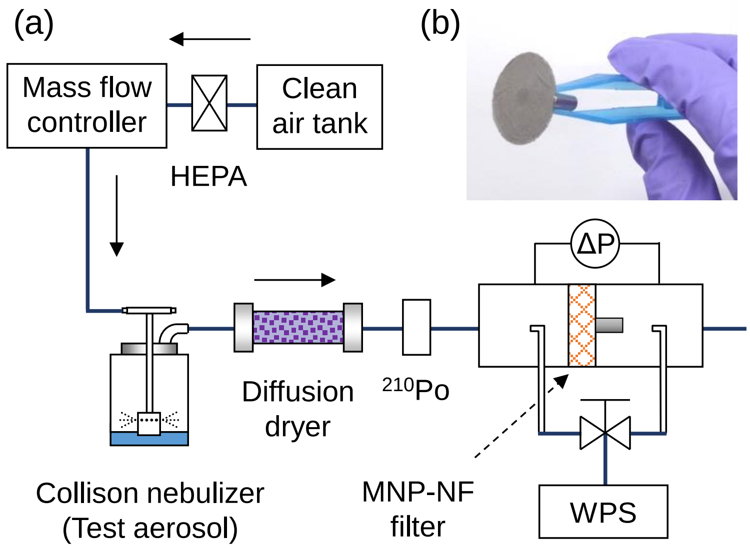

Fig. S1. Filter performance test system. (a) Schematic diagram of the filter performance evaluation system, including the test airborne dust generation system, and (b) picture of a MNP-NF filter with a magnet. Test dust particles were aerosolized from a liquid suspension using a nebulizer stem at a flow rate of 1 L/min with dry, filtered, compressed air. Aerosolized test particles were passed through a diffusion dryer and a ^{210}Po neutralizer to remove moisture and neutralize electrical charges. The test airborne particles were then injected into the filter holder inlet. To evaluate the physical collection efficiency, the particle size distributions and concentrations at the inlet and outlet of the filter holder were measured using a wide-range particle spectrometer (WPS; 1000XP, MSP Corp., Shoreview, USA), which can measure the number concentration of aerosols in the size range from 10 nm to 10 μm. The pressure drop between the upstream and downstream regions of the filter was measured using a micromanometer (FE012; Furness Control, Ltd, Bexill, UK).

Figure S2

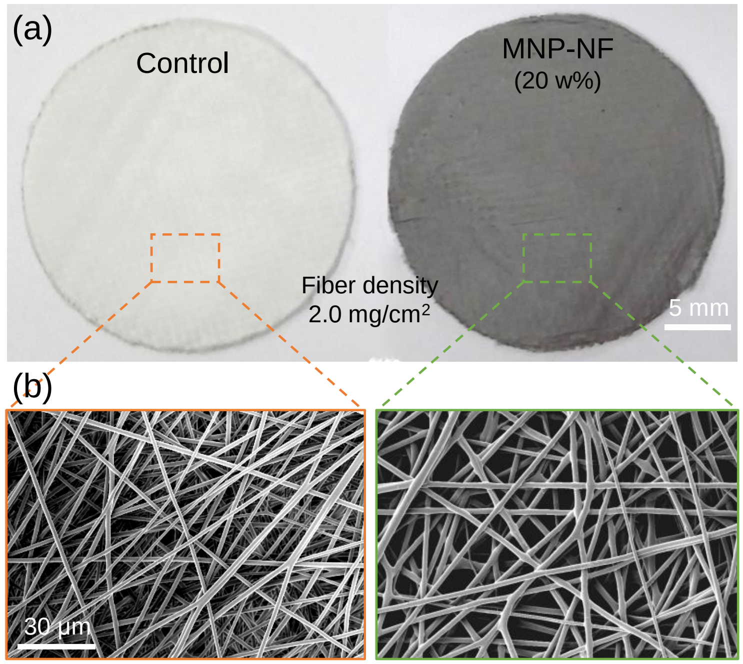

Fig. S2. Comparison between the control filter and MNP-NF filter (20 wt%). (a) Photographs and (b) SEM images of the filters. The prepared filters were weighed using a microbalance (Mettler MT5; Mettler-Toledo International Inc., Seoul, Republic of Korea) with an accuracy of 1 μg. The aerial density of the filters was 2 mg/cm^2.

Figure S3

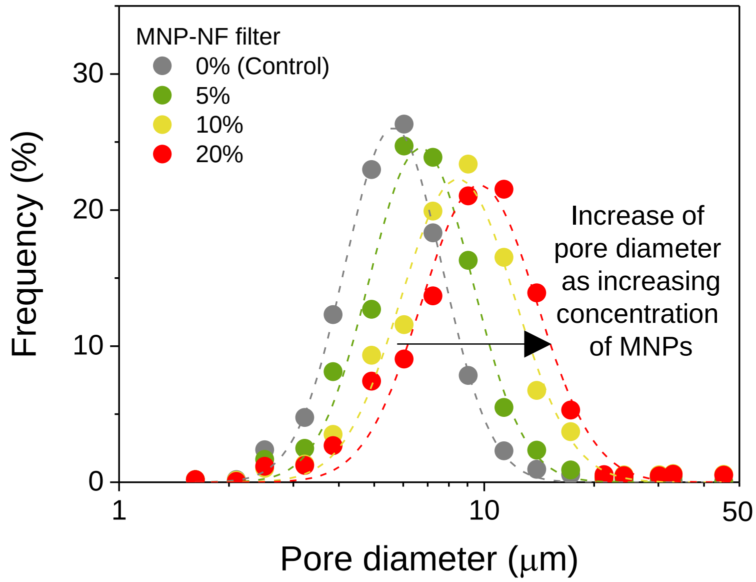

Fig. S3. Pore size distributions of the control and MNP-NF filters. The average pore size of the filter increased with increasing MNP concentration.

Figure S4

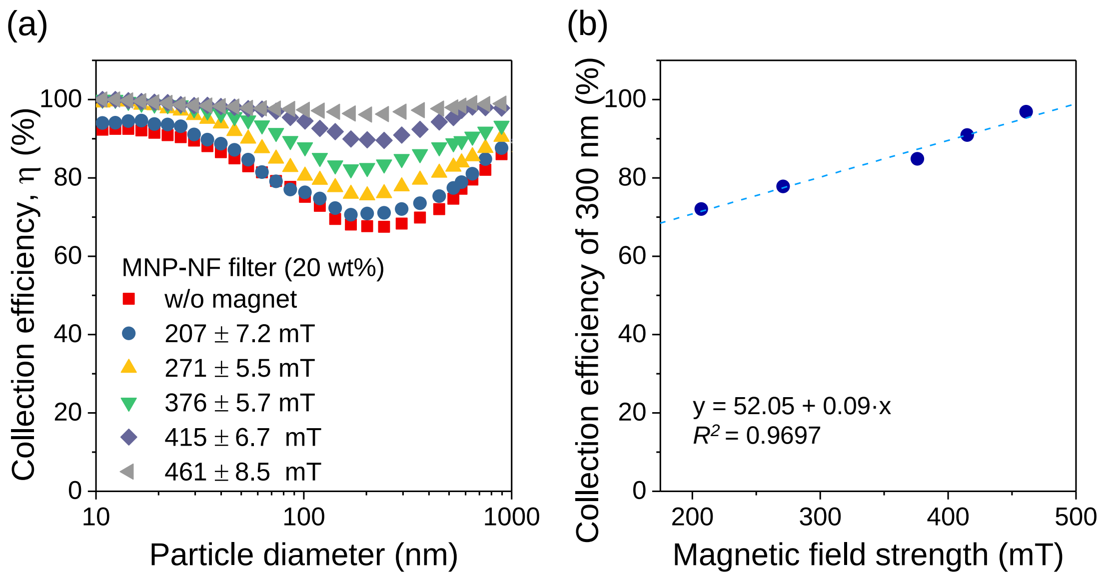

Fig. S4. Filtration performance test of the MNP-NF filter with a range of magnet strengths. (a) Particle collection efficiencies of MNP-NF filter (20 wt%) at a range of magnetic field strengths. (b) Relationship between magnetic field strength and collection efficiency for 300-nm dust particles.

Figure S5

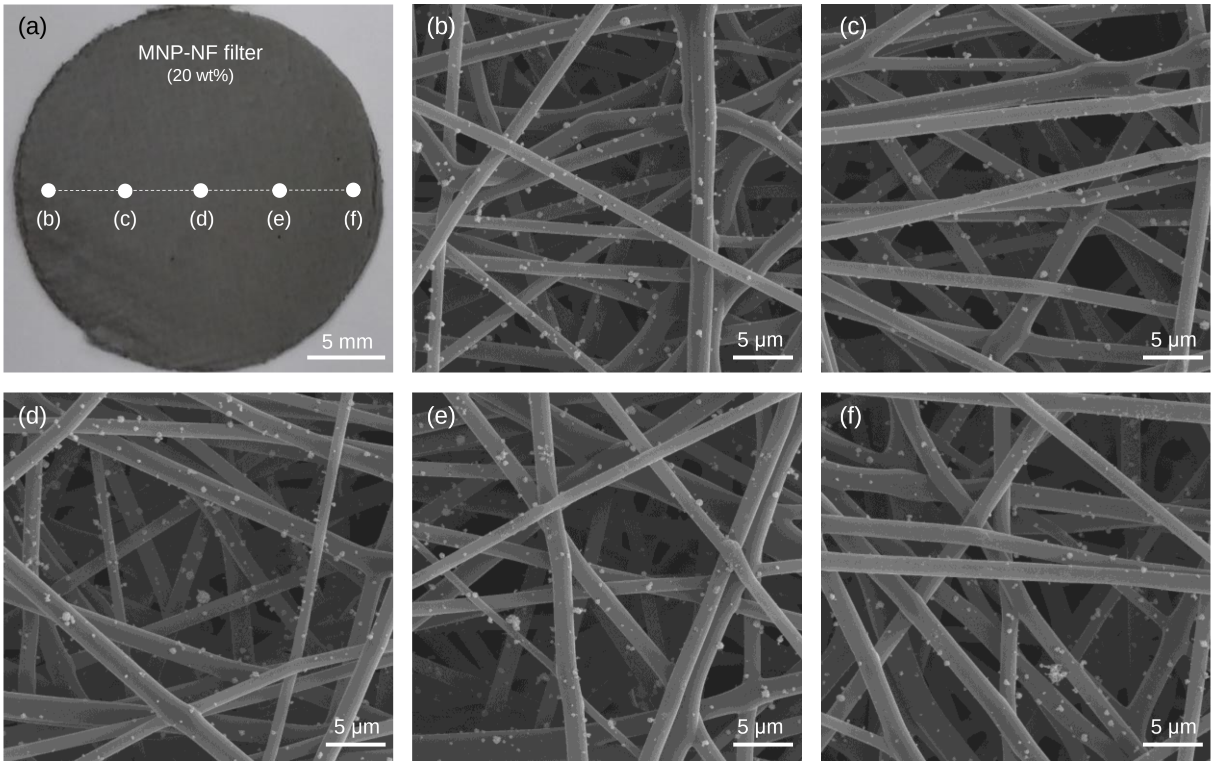

Fig. S5. SEM analysis of the dust-trapped MNP-NF filter. (a) Locations where SEM analysis was performed on the filter. (b–f) SEM images at each location. The metal oxide dusts were completely trapped inside the filter regardless of the location of the filter.

Figure S6

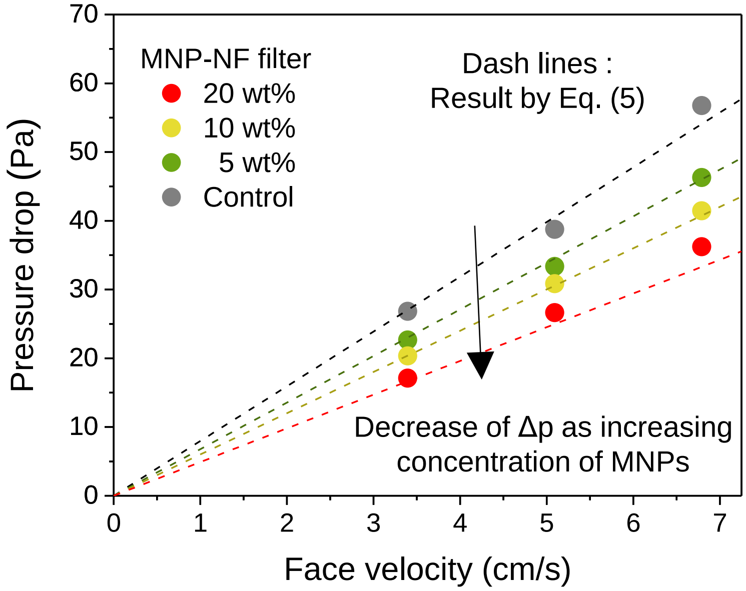

Fig. S6. Relationship between the pressure drop and the face air velocity of the control filter and MNP-NF filters (5, 10, 20 wt%). The filter pressure drop increased with the face air velocity and MNP concentration. In the case of a fibrous filter, the pressure drop, ΔP, can be calculated theoretically in terms of the cumulative drag on the fibers in the filter using the formula $\Delta P = \frac{\sigma t v}{d_f^2}[64\alpha^{1.5}(1+56\alpha^3)]$, where, σ is the air viscosity (1.81 x 10^{-5} Pa·s), t is the filter thickness (m), v is the face velocity (m/s) at the surface of the filter, and d_f is the diameter of the fiber (m).[1] The dotted lines in Figure S6 show the pressure drop calculated using the above theoretical equation. This equation implies that the pressure drop decreases as the fiber and pore size increase.

1. Hinds., W. C. Aerosol Technology: Properties, Behavior, and Measurement of Airborne Particles. (Wiley-Interscience, 1999).

Figure S7

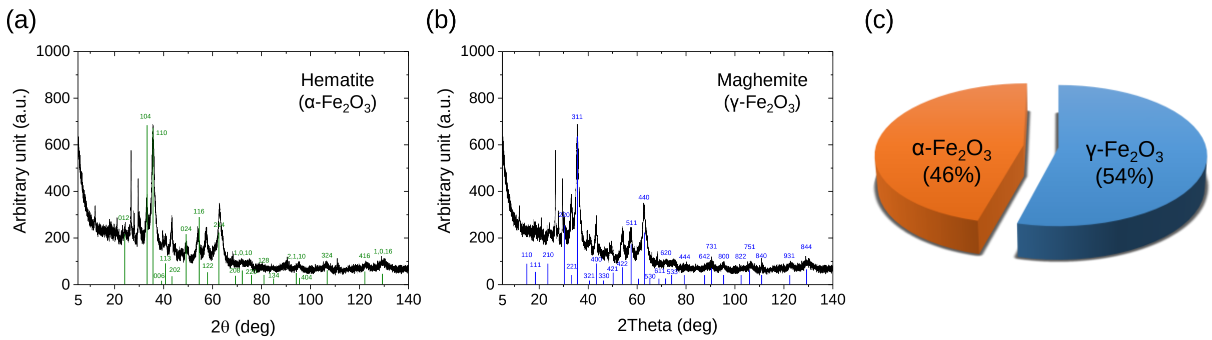

Fig. S7. XRD and RIR quantitative analysis of Fe_2O_3 dust sampled in the subway tunnel. (a) XRD data on α-Fe_2O_3(hematite), (b) XRD data on γ-Fe_2O_3(maghemite), and (c) RIR quantitative ratio of α-Fe_2O_3 and γ-Fe_2O_3. The proportion of α-Fe_2O_3 was found to be 46%, and that of γ-Fe_2O_3 was 54%, in the Fe_2O_3 dust.

Figure S8

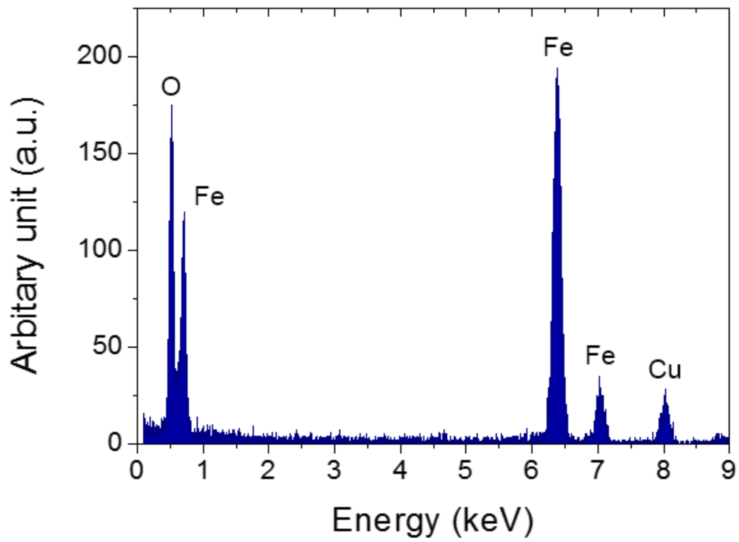

Fig. S8. EDS spectrum of the subway dust. The subway dust exhibited strong peaks at 0.7, 6.4, and 7.0 keV, which indicates the presence of Fe. Owing to the large proportion of Fe in the dust, these peaks were significant compared to those of the other components. This agrees with the result of the XRF analysis in Table S5.